Pergamon

Geochimica et Cosmochimica Acta, Vol. 61, No. 13, pp. 2765–2775, 1997
Copyright © 1997 Elsevier Science Ltd
Printed in the USA. All rights reserved
0016-7037/97 $17.00 + .00

PII S0016-7037(97)00119-1

Oxidation states and ascent history of the Apollo 17 volcanic beads as inferred from metal-glass equilibria

CATHERINE M. WEITZ,* MALCOLM J. RUTHERFORD, and JAMES W. HEAD III
Department of Geological Sciences, Brown University, Providence, Rhode Island 02912, USA

(*Received July* 11, 1996; *accepted in revised form March* 10, 1997)

Abstract—The composition, mode of occurrence, and relationships of metal blebs in the Apollo 17 74001/2 core have been examined to provide insight into variations in oxidation states during ascent and eruption of the lunar volcanic glasses. The 74001/2 core is composed of ~99% orange volcanic glasses and their crystallized equivalents (black beads), with olivine phenocrysts, metal blebs, and, in the upper 8 cm of the core, lithic fragments composing the remaining 1%. In an analysis of this core, twenty-nine metal blebs larger than 4 μm in size were discovered in thin sections taken along the length of the 68 cm deep core. These blebs are classified into three types on the basis of their shape, composition, and distribution. Fourteen of the metal blebs were found trapped inside or between olivine phenocrysts (Type I blebs). Microprobe analyses showed that these spherical blebs have a homogeneous composition of 85% Fe, 14% Ni, and 1.1% Co from core to rim. Six Type II rounded blebs were discovered trapped inside volcanic beads. Their core compositions are similar to the Type I but near the rim these blebs have a sharp decrease in Fe and increase in Ni content. In the lower half of the 74001/2 core where the beads are predominantly black, many contain $\leq$5 μm amoeba-shaped Type III metal blebs. Type III blebs are composed of Fe with trace amounts of Ni. Two angular metal fragments could not be classified into any of the three types. We propose that the Type I blebs formed initially at 4.0 km depth and 1.3 log units below IW at a pressure of 200 bars and a temperature of 1320°C by the formation of C-O gas during graphite oxidation. Once trapped by olivine phenocrysts, the blebs were buffered from further reactions with the melt. The Type II blebs remained in contact with the melt during ascent and experienced loss of Fe to the surrounding melt phase by oxidation reactions which range from 1.3 to 0.9 log below IW. Finally, Type III blebs formed either by exsolution of Fe during crystallization in the fire fountain or by loss of volatiles originally coordinated with Fe to the volcanic gas phase under the reduced conditions in the fountain. *Copyright © 1997 Elsevier Science Ltd*

1. INTRODUCTION AND BACKGROUND

Lunar glasses produced by explosive volcanic eruptions have been identified in samples collected at all six Apollo landing sites. A clod of soil collected at the Apollo 15 site next to Hadley Rille is composed of low-Ti green glasses while soils at the Apollo 17 site in the valley of Taurus-Littrow contain high-Ti orange glasses and their crystallized equivalents (black beads). Regional (>1000 km^2) and localized (<250–550 km^2) dark mantle deposits thought to be composed of submillimeter pyroclastic glasses/beads have also been identified on the Moon, with both deposits generally associated with sinuous rilles or irregular depressions (Gaddis et al., 1985). Because regional deposits are seen on the uplands adjacent to maria, they provide evidence for early explosive volcanism on the Moon that is now covered by younger mare deposits (Head, 1974; Heiken et al., 1974). Theoretical studies by Wilson and Head (1981) suggest that the submillimeter beads may have been produced either in Hawaiian fire fountain or strombolian style eruptions. To be ejected farther than a few kilometers from the vent, theoretical studies (Wilson and Head, 1981; Weitz et al., 1996a) predict that the submillimeter glasses must represent less than 1–2 wt% of the total erupted clasts, implying that most of the clasts are larger in size and land closer to the vent.

Delano (1986) has identified twenty-five suites of pristine glasses after analyses of several thousand glasses from the Apollo samples. The Mg/(Mg+Fe) and Ni content of the glasses are higher than in the basalts, suggesting that the glasses are more primitive and less fractionated than the mare basalts of comparative Ti content (Delano, 1986). Hence, the lunar picritic glasses represent the closest approximation to primary magmas among the mare samples collected (Shearer and Papike, 1993; Longhi, 1987; Delano, 1986). Major element characteristics of the high-Ti magmas and ilmenite melting relationships support a depth of melt segregation for the glasses at 400–500 km where the melt last equilibrated with orthopyroxene and olivine (Green et al., 1975; Delano, 1980; Hess, 1993; Circone and Agee, 1996). Carbon monoxide gas produced by oxidation of graphite is believed to be the dominant gas species driving explosive lunar volcanic eruptions (Sato, 1979; Fogel and Rutherford, 1995), although evidence from condensates on the volcanic beads indicates that other volatiles, including S, Cl, Na, K, and F were involved as well (Meyer et al., 1975; Butler and Meyer, 1976; Wasson et al., 1976; Weitz et al., 1996a). Depending upon the temperature, any graphite suspended in a melt will become out of equilibrium at a given pressure as the magma ascends to the surface. At this pressure, graphite scavenges oxygen from the melt to produce a CO-rich gas phase, with the CO/CO_2 ratio depending upon the temperature and oxygen fugacity (f_{O_2}) (Fogel and

* Author to whom correspondence should be addressed.

Rutherford, 1995). Ni-Fe metal blebs with a surrounding zone of Ni depletion discovered in Apollo 15 low-Ti green glasses represent evidence for in situ formation by reduction, most likely from graphite oxidation (Rutherford and Fogel, 1995).

Upon eruption in the fire fountain, the beads experience different cooling rates related to their size and location in the volcanic plume in a manner similar to that in terrestrial eruptions (e.g., Head and Wilson, 1989). Orange glasses sampled at the Apollo 17 landing site indicate quenching due to rapid cooling that inhibited crystal formation. Other beads with the same composition are black, the result of extensive olivine and ilmenite crystallization. According to Arndt and von Engelhardt (1987), crystallization of olivine followed by ilmenite occurs once the cooling rate of the beads falls below 100°C/s. The texture of the olivines is related to the cooling rate with transitions from dendritic, tabular, acicular, and finally to subequant olivines as the cooling rate is progressively decreased (Heiken and McKay, 1978). In addition, faster cooling rates caused lower Mg/Mg+Fe ratios (Mg*) and an increase in the compositional zonation in olivines of this series.

At the Apollo 17 landing site, a 68 cm deep core (74001/2) was taken on the rim of the 120 m diameter impact crater Shorty. The core consists of orange glasses and their crystallized equivalents (black beads) (Heiken et al., 1974; Heiken and McKay, 1978). The mean size of the orange and black beads is 40 μm (Heiken et al., 1974) and the largest bead identified in the 74001/2 thin sections is a 1.1 mm black bead fragment (Weitz et al., 1996a). Most of the beads are fragmented and fractured either as a result of collisions in the fire fountain or during deposition. Some (<3% volume) olivine phenocrysts and metallic blebs have been identified dispersed throughout the 74001/2 core section (Weitz et al., 1996b). The olivine phenocrysts are interpreted to have formed in the magma during cooling in the conduit prior to the eruption as indicated by their large size, homogeneous composition, the equilibrium (120°) grain boundaries between adjacent faces, and the different texture of these olivines compared to those which nucleated and grew in the black beads.

The Apollo 17 deposit is thought to have been produced from one continuous eruption because the bulk composition of the beads does not change from the bottom to top of the core (Blanchard and Budahn, 1978). Heiken and McKay (1978) observed that the core changed from 76% orange glasses at the top (74002) to 93% black beads at the bottom (74001). Solar and cosmic irradiation studies by Bogard and Hirsch (1978) indicate that the core was inverted by the Shorty Crater impact approximately 10 m.y. ago. Therefore, the original stratigraphy began with deposition of predominantly orange glasses followed by an increasing volume percentage of black beads. Weitz and Head (1995) and Weitz et al. (1996a) proposed that a change in the optical density of the eruption plume from low to high as a result of a decrease in the magma gas content could explain the change from orange to black beads in the 74001/2 core.

In this paper, we have searched for and analyzed metal blebs and associated glasses and olivines in thin sections taken along the length of the 74001/2 core in order to determine the oxidation states during magma ascent and volcanic bead formation, which are of key importance to further understanding the lunar pyroclastic eruption process. After determining the compositions of the blebs, we have divided them into different types and report on the variations in oxidation states implied by their compositions. Our goal is to apply these results to answer the following questions: (1) What is the nature and oxidation state of the source regions that produced the picritic magma? (2) What is the composition of the gas phase which drove the fire fountaining? (3) At what depth did the different gas species exsolve? (4) Can this study of oxidation and gas phase evolution determine the ascent rate for the magma? (5) How did the eruption conditions change with time during the emplacement of the 74001/2 sequence? The answers to these questions will provide further insight into the ascent and eruption of lunar picritic magmas as well as further our understanding of the lunar interior and the volcanic history of the Moon.

2. PROCEDURE AND ANALYTICAL METHODS

Twenty-six thin sections were made along the length of the 74001/2 core, and we have examined all of them with a reflected light microscope searching for metallic blebs. Each thin section is approximately 2.5 cm in length and 1.0 cm wide. The largest bleb identified is 44 μm in diameter, but those found in the volcanic black beads are generally <5 μm in size. Given the limited size resolution of the electron microprobe, we concentrated our study on only those blebs larger than 4 μm. After searching through the thin sections, we have identified twenty-nine metallic blebs larger than 4 μm in size: fourteen are enclosed in or trapped between olivine phenocrysts, fourteen are enclosed in volcanic beads, and one metallic fragment was found by itself. Of the twenty-nine blebs, nineteen were found in the top 33 cm (74002) and ten in the lower 35 cm (74001). In addition to the larger, spherical blebs, we observed that with increasing depth in the core a higher percentage of the black beads contained ≤5 μm amoeba-shaped metallic blebs.

Compositional information for each bleb was obtained using a Cameca Camebax microprobe. Pure Fe, Ni, and Co metal standards were used. A beam diameter of 2 μm was used and traverses were made across the larger blebs at 5–10 μm spacing. Operating conditions were 15 KV and 30 nA. For the smaller blebs (<8 μm) and at the rims of the larger blebs, low totals were renormalized to 100 wt%. Electron microprobe analyses were also made of the large olivine phenocrysts associated with the metal blebs. Finally, compo-

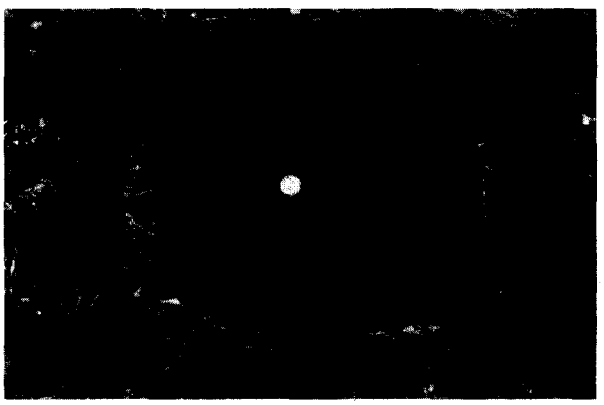

Fig. 1. Reflected light photograph showing an 8 μm metal spherule trapped inside an olivine phenocryst. Surrounding the olivine is crystallized orange glass consisting of smaller olivine and ilmenite crystals.

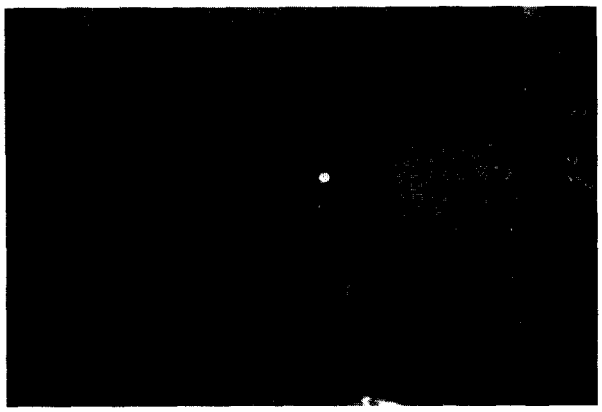

Fig. 2. This 10 μm metal spherule is trapped between three olivine phenocrysts. The olivines are contained inside a partially crystallized orange glass bead that formed as the olivines and magma were erupted and cooled in the fire fountain.

sitional traverses for major elements and Ni were made from the edges of the metal blebs into the surrounding olivines and glass.

3. DESCRIPTION OF METAL BLEBS

3.1. Type I: Fe-Ni Spherules in Olivine Phenocrysts

Fourteen metal blebs are located inside (Fig. 1) or between (Fig. 2) olivine phenocrysts. All of these blebs are perfect spheres. The olivine phenocrysts that entrapped the metal spheres are large (>100 μm), chemically homogeneous euhedral crystals with higher Mg*'s (0.81) than the smaller olivines formed within the beads after the eruption (Mg* 0.78–0.62). In cases where two or more of these olivine phenocrysts occur together in one bead, they have good equilibrium textures with 120° angles between adjacent faces. Microprobe analyses of the largest metal blebs enclosed within olivines indicate that they have a uniform core composition of 85% Fe, 14% Ni, and 1.1% Co by wt% (Fig. 3), with a small decrease in Fe and increase in Ni contents at the rims (Table 1). These small compositional variations at the rims of the blebs most likely result from X-ray excitation in the surrounding olivine. However, one elongated bleb enclosed near the edge of an olivine crystal (Fig. 4) has a very strong change in composition from core to rim (Table 1, #10). At the center of the bleb, the composition is 77% Fe, 21.5% Ni, and 1.4% Co and progresses to 65.3% Fe, 33.2% Ni, and 1.5% Co towards the rims. The double hump in Fe and Ni contents at the center of the elongate bleb (Fig. 3) may indicate that the bleb represents two coalescing spheres; this idea is supported by a small decrease in the width of the bleb near the center producing a boudin shape. Less than one micron separates this elongated bleb from another round metal bleb with a significant decrease in Fe and increase in Ni at the rim (Table 1, #9). Because this rounded bleb has a strong reaction rim, and it is adjacent to the elongated bleb, it may indicate that the blebs remained in contact with the melt and experienced further and variable oxidation before they were entrapped within the olivine. Support for this statement includes the fact that these blebs are located at the edge of the olivine, indicating that they were trapped nearer the end of the olivine phenocryst growth event than a metal spherule located closer to the center of the same olivine which shows no reaction rim. Finally, many of the smaller blebs have core compositions with slightly lower Fe and higher Ni contents than the larger blebs (Table 1). Because the core compositions of the smaller blebs match the rim compositions of the larger blebs, the smaller blebs may simply represent the rims of larger blebs that were cut along the edge during the process of making thin sections.

Compositional traverses away from the blebs and into the adjacent olivines show no variation in Mg, Fe, and Ni contents that can be attributed to a metal bleb formation process. Therefore, we favor metal bleb formation followed by olivine capture with no later reactions occurring within the blebs during ascent. Depending upon when the bleb was captured and enclosed within the olivine during ascent, its composi-

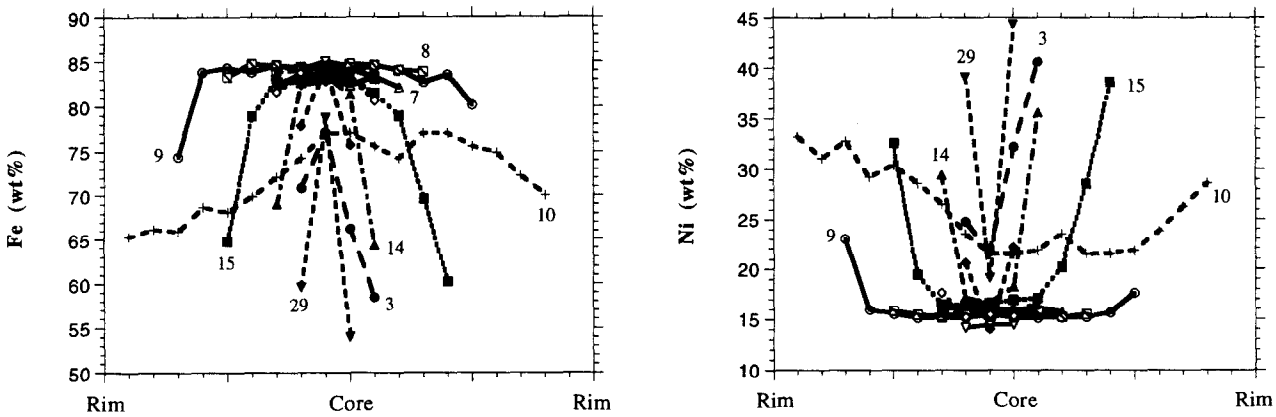

Fig. 3. Iron and nickel transects across the metal blebs. The Fe-Ni spherules found trapped inside or between olivine phenocrysts have relatively homogeneous compositions of 85% Fe, 14% Ni, and 1.1% Co by weight from core to rim (open symbols). In contrast, the Fe-Ni blebs trapped within volcanic beads (solid symbols) show strong reaction rims indicating a decrease in Fe and increase in Ni content in traverses approaching the rim. An elongate bleb inside an olivine (crosses) shows a double hump in a traverse along its length, possibly representing two coalescing spheres with reaction rims (see Fig. 4). The distance between each analysis point is 8 ± 3 μm. Numbers refer to bleb numbers listed in Table 1.

Table 1. Traverses across the metal blebs showing their compositions.

Bleb num.	Thin section**	Bleb type	Fe (wt%)	Co (wt%)	Ni (wt%)	Total	Location	Size (μm)
1	2,6027	I	82.4	1.0	15.7	99.1	rim	12
			82.8	1.2	15.6	99.6	core	
			83.1	1.0	15.9	100.0*	rim	
2	2,6028	I	81.6	1.2	17.6	100.4	rim	44
			83.7	1.2	15.2	100.1		
			83.5	1.1	15.4	100.0	core	
			83.4	1.2	15.3	99.9		
			80.6	1.2	16.8	98.6	rim	
3	2,6029	II	70.8	1.4	24.7	96.9	rim	22
			77.1	1.5	21.7	100.3	core	
			66.2	1.3	32.2	99.7		
			58.4	1.0	40.6	100.0*	rim	
4	2,6029	I	83.8	0.9	15.6	100.3	rim	26
			84.1	1.1	15.6	100.8		
			83.4	1.1	15.2	99.7	core	
			84.3	1.1	15.6	101.0		
			83.1	1.0	15.8	99.9	rim	
5	2,6030	II	52.3	0.9	46.7	99.9*		8
6	2,6031	I	83.1	1.1	15.5	99.7		8
7	2,0631	IV	83.3	1.2	15.8	100.3	rim	32
			84.7	1.1	15.4	101.2		
			84.6	1.2	15.3	101.1		
			84.4	1.2	15.4	101.0		
			84.5	1.2	15.5	101.2	core	
			84.7	1.1	15.3	101.1		
			84.6	1.1	15.6	101.3		
			84.0	1.1	15.2	100.3		
			83.9	1.1	15.5	100.5	rim	
8	2,6031	I	82.7	1.1	16.0	99.8	rim	18
			82.7	1.1	16.1	99.9		
			83.5	1.1	16.0	100.6	core	
			82.3	1.1	15.9	99.3	core	
			83.3	1.1	16.1	100.5		
			82.1	1.1	15.7	98.9	rim	
9	2,6031	I	74.4	1.5	23.0	98.9	rim	22
			83.8	1.3	15.9	101.0		
			84.3	1.2	15.5	101.0		
			83.8	1.1	15.1	100*		
			84.6	1.1	15.1	100.8		
			84.1	1.1	15.1	100.3	core	
			84.3	1.2	15.5	101.0	core	
			83.8	1.1	15.1	100.0*		
			84.6	1.1	15.1	100.8		
			84.1	1.1	15.1	100.3		
			82.7	1.1	15.2	99.0		
			83.5	1.1	15.6	100.2		
			80.1	1.4	17.6	99.1	rim	
10	2,6031	I	65.3	1.5	33.2	100.0*	rim	32
			66.1	1.5	31.1	98.7		
			65.9	1.3	32.8	100.0*		
			68.7	1.4	29.2	99.3		
			68.1	1.4	30.4	99.9*		
			69.9	1.5	28.6	100.0*		
			72.1	1.4	26.5	100.0*		
			74.2	1.3	23.5	99.0		
			77.0	1.4	21.5	99.9	core	
			77.0	1.4	21.5	99.9	core	
			75.5	1.4	21.8	98.7		
			74.2	1.3	23.5	99.0		
			77.0	1.4	21.5	99.9		
			77.0	1.4	21.5	99.9		
			75.5	1.4	21.8	98.7		
			74.8	1.4	23.8	100.0*		
			72.2	1.5	26.3	100.0*		
			70.0	1.4	28.6	100.0*	rim	
11	2,6032	III	99.7	0.0	0.3	100.0*		5
12	2,6032	I	83.7	1.1	14.7	99.5		10

Table 1. (Continued)

Bleb num.	Thin section**	Bleb type	Fe (wt%)	Co (wt%)	Ni (wt%)	Total	Location	Size (μm)
13	2,6034	III	99.7	0.0	0.3	100*		8
14	2,6034	II	69	1.4	29.4	99.8	rim	13
			82.6	1.2	17.1	100.9		
			83.5	1.1	16.5	101.1	core	
			81.3	1.2	18.2	100.7		
			64.3	1.3	35.6	101.2	rim	
15	2,6034	II	64.7	1.3	32.6	98.6	rim	30
			78.9	1.3	19.4	99.6		
			83.0	1.1	16.4	100.5		
			82.8	1.2	16.4	100.4		
			83.6	1.2	16.6	101.4	core	
			83.0	1.1	16.9	101.0	core	
			81.5	1.1	17.1	99.7		
			78.9	1.3	20.2	100.4		
			69.6	1.4	28.5	99.5		
			60.2	1.2	38.6	100.0*	rim	
16	2,6035	II	77.8	1.5	20.6	99.9*	rim	15
			84.2	1.2	14.0	99.4	core	
			75.7	1.4	22.1	99.2	rim	
17	2,6035	I	84.1	1.0	14.1	99.2	rim	16
			85.0	1.2	14.4	100.6	core	
			84.5	1.1	14.4	100.0	rim	
18	2,6035	I	53.5	1.3	45.2	100.0*		6
19	1,6026	III	99.8	0.0	0.2	100.0*		5
20	1,6027	I	87.2	0.6	12.2	100.0*		6
21	1,6029	I	82.3	1.1	15.1	98.5	rim	20
			83.6	1.1	15.4	100.1		
			83.1	1.1	15.3	99.5	core	
			84.1	1.1	15.6	100.8		
			83.3	1.2	15.5	100.0*	rim	
22	1,6029	I	79.9	1.3	18.8	100.0*	core	10
23	1,6030	III	100.0	0.0	0.0	100.0*		4
24	1,6030	III	100.0	0.0	0.0	100.0*		4
25	1,6031	I	82.1	1.2	16.7	100.0*		8
26	1,6031	III	99.4	0.2	0.4	100.0*		6
27	1,6033	III	99.6	0.0	0.4	100.0*		4
28	1,6036	IV	97.6	0.0	0.9	98.5		6
29	1,6036	II	59.6	1.3	39.1	100.0*	rim	16
			78.7	1.3	19.1	99.1	core	
			54.0	1.0	44.3	99.3	rim	

* Normalized to 100 wt%.
** 2,6027 is actually 74002,6027 located at the top of the core while 1,6036 is 74001,6036 located at the bottom of the core.

tion will reflect the last oxidation state of the melt-metal equilibrium.

3.2. Type II: Fe-Ni Blebs in Volcanic Beads

Six rounded metal blebs were found trapped within volcanic beads away from olivine phenocrysts. While most of these metal blebs are spherical, several show rounded but nonspherical shapes (Fig. 5). One of the blebs is situated adjacent to an olivine phenocryst but is surrounded by orange glass (Fig. 6). The glass has partially crystallized olivine and ilmenite within a few microns of the contact with the olivine phenocryst, and the bleb is located within this partially crystallized zone. Another elongated bleb is located in an orange glass fragment that had partially crystallized into linear olivines and ilmenite. The bleb is situated in the orange glass adjacent to a linear olivine crystal. The other five metal blebs were located in crystallized orange glasses (i.e., black beads). The dominance of metal spheres in black beads rather than orange glasses is most likely related to the fact that the majority of beads in the 74001/2 section are crystallized black beads.

The metal blebs in the black and orange beads have core compositions that approach or are equivalent to the blebs trapped in olivine phenocrysts (Table 1). Compositional traverses across the blebs trapped in the beads show them to have Ni-rich, Fe-poor rims (Fig. 3). The composition of the rims analyzed range from 77.8% Fe, 20.6% Ni, and 1.5% Co to 52.3% Fe, 46.7% Ni, and 0.9% Co by weight. The zoning to more Ni-rich rims is always progressive, but the zone thickness varies from 5–20 μm in the different blebs. Some of the variability in rim composition is due to differences in beam emplacement during analysis, but many of the rim compositional differences shown in Fig. 3 are real. Compositional traverses for Fe and Ni from the edge of the metal bleb into the surrounding orange glass show no

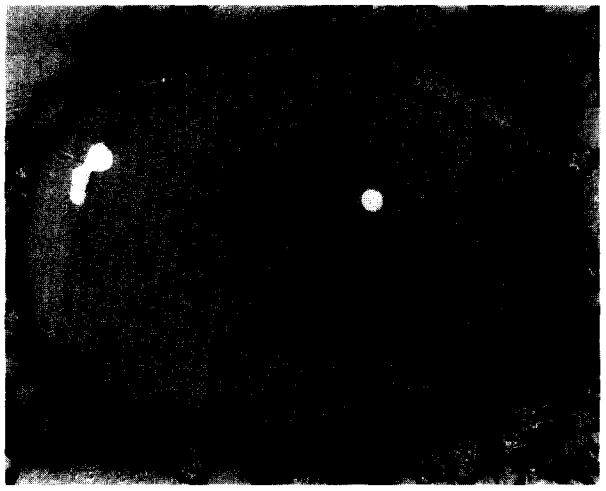

Fig. 4. Three metal blebs can be seen trapped inside this olivine phenocryst. The metal spherule to the right is approximately 20 μm in diameter and it has a homogeneous composition of 85% Fe, 14% Ni, and 1.1% Co by weight. In contrast, the two metal blebs located at the edge of the olivine to the left are not perfect spherules and have reaction rims showing a decrease in Fe and increase in Ni content from core to rim. The elongate bleb may represent two coalescing blebs because it has a decrease in width towards the center, and its composition shows a double hump in Fe and Ni content at the center (see Fig. 3).

detectable variations in the glass composition which would complement the zonation in the enclosed metal blebs. This observation contrasts with the nickel depletion zones adjacent to Ni-rich metal blebs in the low-Ti Apollo 15 green glasses (Rutherford and Fogel, 1995). The different composition of the metal blebs in the volcanic beads (85:14 vs. 15:85 wt% Fe:Ni in the orange and green glasses, respectively) and their rim zonation both indicate a somewhat different origin from that proposed by Rutherford and Fogel (1995) for the green glass metal blebs. In addition, the present nonspherical shape of the metal blebs in the volcanic beads supports some form of rim alteration process occurring after their formation.



Fig. 5. Two rounded Type II metal blebs trapped inside a 130 μm diameter black bead. Unlike the Type I blebs, the Type II are not perfect spheres in shape, and they have sharp decreases in Fe and increases in Ni content from core to rim. The bright, linear crystals interspersed throughout the bead are ilmenite, and the larger, darker crystals are olivine in this reflected light photograph.

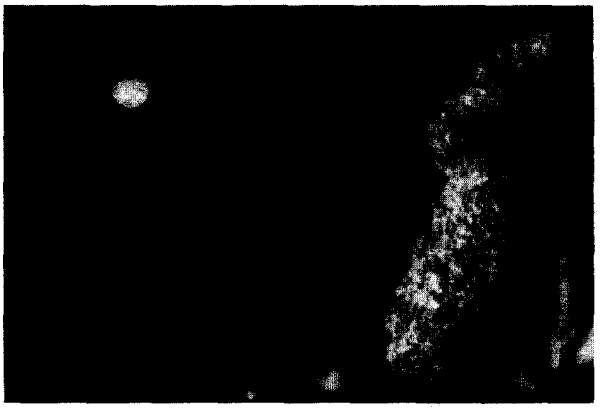

Fig. 6. Reflected light photograph showing a 15 μm metal spherule situated adjacent to an olivine phenocryst fragment in partially crystallized glass. The olivine is to the left and the orange glass is to the right.

3.3. Type III: Fe Blebs in Black Beads

A higher percentage of the volcanic beads were found to contain very small ($\leq$5 μm) irregularly-shaped metal blebs in samples further down the core where the black beads dominate (74001). These metal blebs have finger-like projections and resemble amoebas in appearance (Fig. 7). The blebs are located in the residual glass matrix and are randomly distributed throughout the beads. Microprobe analy-

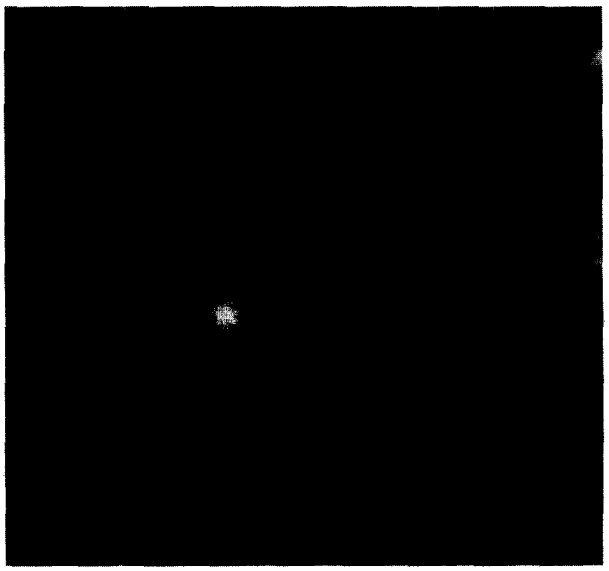

Fig. 7. Type III amoeba-shaped bleb (arrow) located inside a black bead fragment. The bleb is approximately 9 μm in size, and it has a composition of Fe with trace amounts of Ni.

ses of the amoeba-shaped blebs larger than 4 μm in size show that they are composed of Fe with trace amounts of Ni (Table 1). However, their small size and irregular shape make it impossible to obtain a high total wt% metal. The Fe-rich blebs were never identified in orange glasses or the large olivine phenocrysts. The strong association between the amoeba-shaped Fe-rich blebs in black volcanic beads that had large olivines, spinel, and ilmenite crystals suggests that the iron blebs form only after significant crystallization had occurred within the bead.

3.4. Type IV: Metal Fragments

In addition to the metal blebs described previously, we also identified two metal fragments that could not be classified into any of the other three types of blebs. One 32 μm metal fragment had a composition similar to that of the Type I blebs (Table 1, #7), but it was jagged in shape and was enclosed in neither an olivine phenocryst nor a volcanic bead. Most likely the bleb was dislodged from an olivine phenocryst either during a collision in the fire fountain or after deposition onto the lunar surface. The second metal fragment was rectangular in shape, 6 × 4 μm in size, and was located in a volcanic bead fragment. It has a composition of 97.6 wt% Fe and 0.9 wt% Ni (Table 1, #28), which is similar to that of the Type III blebs, although the Ni content is higher. However, its rectangular shape does not resemble that of any of the Type III blebs, and, therefore, we have not classified it as Type III.

4. DISCUSSION

4.1. Origin of the Metal Blebs

The uniform composition of the metal blebs trapped within and between olivines (Type I) indicates that an olivine-metal-melt equilibrium developed either in a magma storage zone or in the conduit during ascent of the magma. Rutherford and Fogel (1995) proposed that Fe-Ni metal blebs (15 wt% Fe, 85 wt% Ni) enclosed in Apollo 15 green glasses originated when carbon present in the ascending magma reached a pressure which required its conversion to a CO-rich gas and a concurrent reduction of FeO and NiO in the melt phase to form the metal. They found Ni depleted halos in the glass surrounding the metal blebs to support this hypothesis. A similar process is considered to have operated in the orange glass magma (Sato, 1979) and other basalt-like lunar melts (Colson, 1993). While it is possible that the metal blebs came up with the magma from depth and re-equilibrated with the melt as the pressure and temperature decreased, several points argue against this possibility. The carbon oxidation process is the only process we know which could have caused a metal reduction to occur simply because the pressure on this magma was reduced during magma ascent (Fogel and Rutherford, 1995); loss of S has been ruled out by calculations by Sato (1976). In addition, the preservation of compositional zonation within metals trapped in olivine (Table 1, #9) suggests a short time between entrappment and eruption; a longer repose time at magmatic temperatures would have allowed homogenization by diffusion in the 20–40 μm blebs (Heyward and Goldstein, 1973). Finally, the fact that the metal spherules are associated with explosively erupted gas-rich magma and undergo changes in composition during the eruption indicates that their origin is linked to oxidation/reduction processes during gas formation.

The main gas phase component produced in the reduction process to form the metal blebs is considered to be CO according to the following reactions:

$$FeO + C \rightarrow Fe^0 + CO \quad (1)$$

$$NiO + C \rightarrow Ni^0 + CO \quad (2)$$

In addition, the reduction of FeS dissolved in the melt to produce a sulfur species in the gas phase may have contributed to metal bleb formation by the following reactions:

$$FeS\,(melt) + 0.5O_2\,(melt) \rightarrow Fe^0\,(metal) + SO\,(gas) \quad (3)$$

$$FeS\,(melt) + CO\,(melt) \rightarrow Fe^0\,(metal) + COS\,(gas) \quad (4)$$

However, calculations by Sato (1976) indicate that fugacities of the S species under lunar conditions would have been very low and inadequate to drive a fire fountain process. In contrast, Fogel and Rutherford (1995) have shown that sufficient amounts of CO gas can be produced by oxidation of graphite to account for the volatiles that drove the explosive lunar eruptions that produced the dark mantle deposits. Therefore, we favor oxidation of graphite and production of CO-rich gas as the origin of the metal blebs.

The metal blebs trapped in olivine phenocrysts shortly after their formation experienced no further reactions during ascent in the conduit (Fig. 8). However, in one example (Fig. 4) we have identified metal blebs with reaction rims enclosed within an olivine phenocryst. The metal spherule trapped at the center of the olivine shows no reaction rim presumably because the bleb was trapped shortly after formation by the growing olivine. The other metal blebs, including a rounded bleb and an adjacent elongate bleb both located near the edge of the phenocryst, have reaction rims because they were trapped by the olivine later, after having experienced further reactions with the melt. The spherical shape of the Type I metal blebs is considered to be due to the high surface tension between solid Fe-Ni metal and basaltic melt. At the liquidus temperature of this magma (1320°C), metal of this composition had to be solid unless it contained large amounts of S or C. It would take >20 m%S or >5 m%C to lower the melting point of Fe to 1320°C (Hansen, 1958). These levels of S and C, which could be detected analytically, have not been observed.

The Fe-Ni blebs contained within volcanic beads (Type II) show a decrease in Fe and an increase in Ni content from core to rim. Because their core compositions are very similar, these blebs probably began with the same composition as the metal spherules trapped in the olivine phenocrysts. However, because the Type II blebs remained in contact with the melt, they experienced further reactions under more oxidizing conditions during ascent in the conduit (Fig. 8). Assuming the melt in equilibrium with the metal was the same before and after the change in metal composition, the more oxidizing conditions are required by the Ni-rich rims and the high f_{O_2} of the $Ni + 0.5O_2 \rightarrow NiO$ equilibrium relative to the $Fe + 0.5O_2 \rightarrow FeO$ equilibrium.

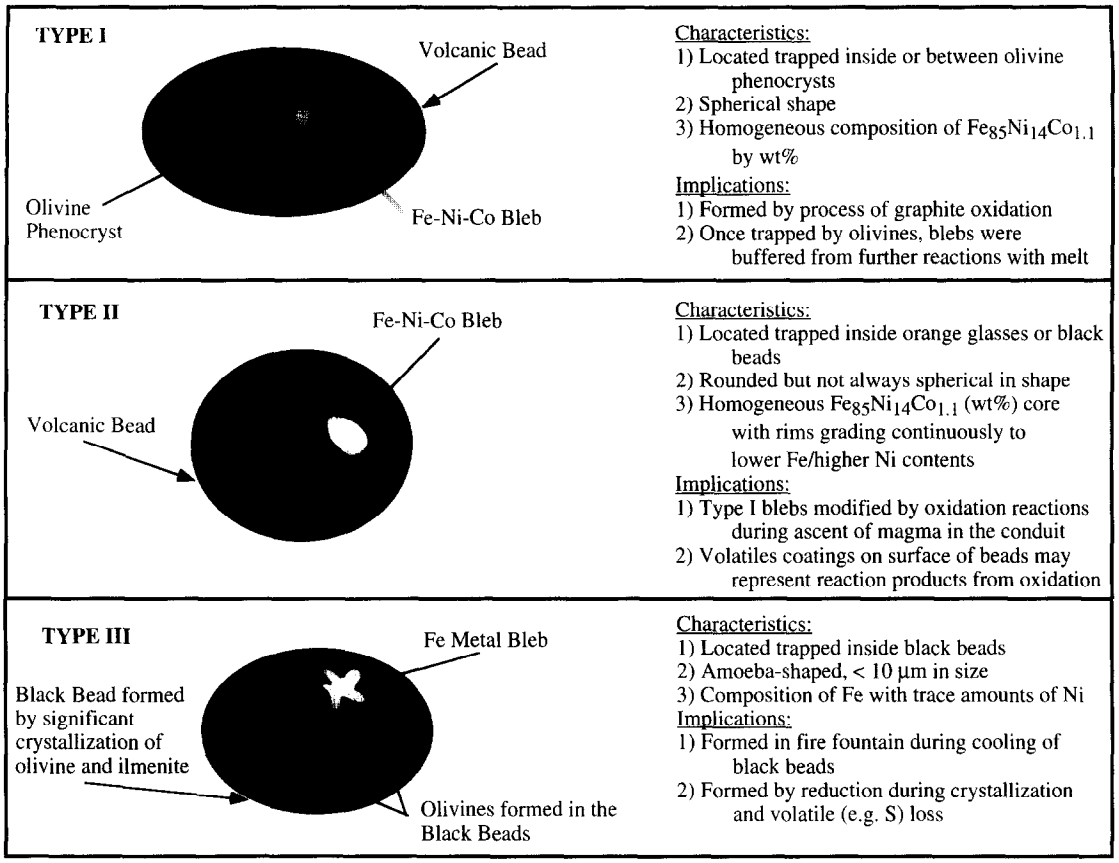

Fig. 8. Diagram illustrating the characteristics and implications for the three types of metal blebs identified in the 74001/2 core.

The somewhat irregular outline of the Type II blebs and the fact there is no noticeable change in Ni content in the melt (glass) in traverses away from the blebs suggest the rim development involved an oxidation of Fe from the metal spherule rather than a reduction of NiO. There are several reactions that we propose may have caused oxidation of the Type II blebs during ascent based upon studies of surface coatings on the beads. Volatile elements including Na, Zn, S, Cl, F, P, and K have been identified as primary components of these coatings (Meyer et al., 1975; Butler and Meyer, 1976; Wasson et al, 1976; Weitz et al., 1996b). The elements are thought to represent volatiles released during the fire fountain eruption that later recondensed on the surfaces of the volcanic beads. Presumably these elements would have originally been coordinated with oxygen in the melt before they were released to the gas phase during the eruption. The result of their release would be an oxidation of the remaining metal-melt assemblage by any of the following reactions:

$$Fe^0 + Na_20 \rightarrow FeO + Na \quad (5)$$

$$Fe^0 + K_2O \rightarrow FeO + K \quad (6)$$

$$5Fe^0 + P_2O_5 \rightarrow 5FeO + 2P \quad (7)$$

$$Fe^0 + ZnO \rightarrow FeO + Zn \quad (8)$$

$$Fe^0 + COS \rightarrow FeO + CO \quad (9)$$

The complex composition of the condensates on the surfaces of the black and orange volcanic beads indicates that a number of these reactions took place during growth of the volcanic gas phase. However, it is not known whether this part of the gas production process was controlled by gas and melt equilibrium or by the kinetics of cation diffusion and exchange at the melt-gas interface. The process must have begun shortly after the C was oxidized to produce the CO-rich gas, however, and before the explosive eruption began because some partly oxidized (Type II) blebs were trapped in the final stages of olivine phenocryst growth, and this growth occurred prior to the explosive ascent.

We propose that the amoeba-shaped Fe-rich blebs (Type III) formed in heavily crystallized black beads during cooling in the fire fountain. If metal can dissolve in silicate melts (e.g., Colson, 1992), then crystallization of the melt would eventually cause a metal-phase separation, in this case resulting in Fe blebs. However, recent studies (Dingwell et al., 1994; Holzheid et al., 1994) find no evidence supporting metal solubility. Therefore, the origin of the Type III blebs in the black beads is best explained by loss of elements, such as dissolved S, during crystallization of the orange glasses in the fire fountain (Fig. 8). Support for this origin includes the fact that these elements are speciated with Fe

in the melt, they are volatile and present in the lunar volcanic gas, and they are still present in small but variable amounts in the orange glass.

4.2. Oxidation States and Depth of Formation

Assuming that metal reduction was due to graphite oxidation to form a CO-rich gas, a process which occurs when the pressure on graphite-bearing magma is decreased and CO becomes more stable than graphite (Fogel and Rutherford, 1995), we have calculated the f_{O_2} for the orange glass magma during metal bleb formation. Using the composition of the 74220 orange glass reported by Delano (1986), we have calculated the molar composition for each oxide. In the case of FeO, the mole fraction (X_{FeO}) is 0.195. From Doyle (1989) we calculate an activity coefficient for FeO of 1.0 $\pm$ 0.2 for a basaltic melt of orange glass composition at 1600K and -11.92 log f_{O_2}. The activity of FeO (a_{FeO}) is thus simply equal to the mole fraction of FeO, 0.195. For Fe-Ni metals with $\geq$85 wt% Fe, the activity coefficient for Fe in the blebs is equal to 1.0 (Rammensee and Fraser, 1981), and hence $a_{Fe} = X_{Fe} = 0.85$ in the Fe-Ni metal blebs. Finally, the f_{O_2} can be expressed as a function of a_{FeO} and absolute temperature (T) (e.g., Doyle, 1989) by

$$a_{FeO} = a_{Fe} f_{O_2}^{0.5} \exp(28719.2/T - 5.837) \quad (10)$$

For the Fe-Ni metal blebs trapped inside olivines, we use a core composition of 85% Fe by weight and a liquidus temperature of 1593 K at 0 bars (Green et al., 1975) to calculate an f_{O_2} of 1.35×10^{-12} for the metal sphere-melt equilibrium in the orange glass magma. The f_{O_2} for the iron-wustite (IW) equilibrium at this temperature is 2.57×10^{-11}, yielding an f_{O_2} of 1.3 $\pm$ 0.2 log units below IW for the metal blebs trapped in olivine.

In the case of Fe-Ni metal blebs entrapped within volcanic beads, some reaction after formation caused either the amount of Fe to decrease or the Ni content to increase at the rims. The reaction that removed Fe relative to Ni is preferred because of the nonspherical shape of the blebs and the fact that there is no depletion in the NiO content of the glass surrounding the grains. The oxidation of Fe to form FeO in the melt surrounding these blebs would cause an FeO increase too small to be detected in the FeO-rich melt. If we assume the same 1593K temperature for the melt and take the lowest Fe of 52.3 wt%, we calculate an f_{O_2} of 3.36×10^{-12} or 0.9 log units below IW at the time of final melt re-equilibration with these metal blebs. Therefore, as the magma ascended in the conduit, it experienced further reactions which produced more oxidizing conditions. Although it should be theoretically possible to perform a similar calculation of f_{O_2} from the Ni distribution (Snyder and Carmichael, 1992), we found that because Ni is a trace element in the magma and the activities for Ni and NiO are not as well known as they are for Fe, we could not obtain a reasonable value for f_{O_2} using Ni. For example, using X_{NiO} of 5.43×10^{-3} (Delano, 1986), an activity coefficient of 0.63 for Ni (Rammensee and Fraser, 1981), a_{Ni} equal to 0.086, and assuming an activity coefficient of 1.0 for NiO since it is a trace element, we calculate an f_{O_2} of 1.18×10^{-9} from equations by Hemingway (1990) and Snyder and Carmichael (1992).

If the formation of the initial Type I metal spherules was caused by graphite oxidation, then the graphite-gas equilibrium calculations can be used in conjunction with the metal-melt estimates to determine the depth of gas phase production. Rutherford and Fogel (1995) calculated an f_{O_2} of 0.9 log units below IW at 1420°C and a 12 km depth for the formation of Fe-Ni blebs in the low-Ti green glasses. For the orange glasses, the f_{O_2} of 1.3 log units below IW at 1320°C yields a pressure of 200 bars at the graphite oxidation surface (Fig. 9). The formation depth for the orange glasses using this pressure and 20 km/kbar for the Moon yields a critical depth of 4.0 km for the formation of the C-O gas phase and the Type I metal blebs. Sato (1979) used the solid-electrolyte method to obtain an f_{O_2} (-10.70 log units) only slightly below IW at 1325°C for the orange glass magma. This is equivalent to a pressure of about 700 bars at the intersection with the graphite-gas equilibrium (Sato, 1979), which is significantly greater than the 200 bars we calculate based on the metal-melt equilibria. However, the intrinsic f_{O_2} yielded by the Sato (1979) experiments may have been influenced by coatings on the glass, and he also found that an irreversible ($\sim$1 log unit) reduction occurred as his experiment exceeded about 1150°C. Therefore, we believe that the f_{O_2}'s calculated from the metal-silicate equilibria are more reliable. It should also be noted that our results indicate a very reduced state after graphite oxidation (Type I bleb formation) followed by more oxidizing conditions as the magma ascended (Type II bleb formation). Finally, conditions in the fire fountain during black bead formation indicate a more reduced state resulting in formation of Type III metal blebs.

4.3. Implications for the Ascent and Eruption of the Pyroclastic Glasses

Based upon multisaturation experiments (Green et al., 1975; Hess, 1993), the high-Ti orange glass melt appears

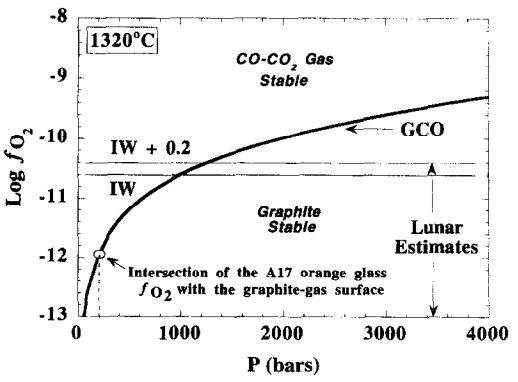

Fig. 9. Oxygen fugacity of the graphite-CO oxidation surface (GCO) as a function of pressure at 1320°C. Typical estimates for the lunar interior f_{O_2} range from IW + 0.2 to IW $-$ 2.5. The f_{O_2} of 1.3 units below IW for the orange glasses is obtained for Fe equilibrium between the Type I metal blebs and the coexisting melt (see text). This f_{O_2} yields a corresponding critical pressure of CO gas formation at 200 bars, or 4.0 km depth in the lunar crust.

to have segregated from its source at 400–500 km depth. However, Longhi (1992) has argued that the low-Ti picritic glasses may have been produced over a range of depths by polybaric melting and that a similar melting mechanism may have produced the high-Ti melts. After passing through the crust-mantle boundary, the melt became negatively buoyant but was still able to ascend due to overpressurization (Head and Wilson, 1992). As shown above, at 200 bars and 4.0 km depth, graphite suspended in the magma was no longer stable and oxidized to produce CO gas and Fe-Ni-Co metal blebs. After metal bleb formation, small-scale adiabatic cooling in the melt allowed some olivine phenocrysts to form.

We can use the sizes of the metal blebs and olivine phenocrysts to estimate the minimum rise speed of the melt during ascent in the conduit after their formation. The largest metal spherule has a diameter of 44 μm and the largest olivine phenocryst is approximately 600 μm in diameter. These sizes represent minima because it is very unlikely that the thin sections are cut exactly through the center of these features, and, in the case of the olivine phenocrysts, many appeared fragmented. Stokes Law for crystal settling is:

$$\nu = \frac{2gR^2(\rho_m - \rho_c)}{9\eta} \quad (11)$$

where ν is the settling velocity, g is the accelaration due to gravity, R is the radius of the crystal, η is the viscosity of the melt, and ρ_m and ρ_c are the densities of the melt and crystal, respectively.

Assuming a density of 3.0 g/cm^3 for the magma (Delano, 1990), a density of 7.87 g/cm^3 for the Fe-Ni metal spheres, a density of 3.5 g/cm^3 for olivine, a viscosity of 4.1 Poise for the magma (Delano, 1990), and radii of 22 and 300 μm for the metal spheres and olivines, respectively, we calculate a settling velocity of 2.0×10^{-4} cm/s or 0.74 cm/hr for the metal blebs and 3.9×10^{-3} cm/s or 14.0 cm/hr for the olivine phenocrysts. Therefore, as long as the magma did not stall or slow down for a significant period of time, the blebs and olivines could be carried from depth in the course of the eruption. Because no olivine phenocrysts are associated with the green glasses (Delano, 1979), they may have had a faster ascent rate or a higher (superliquidus) magma temperature during ascent in the conduit compared with the orange glasses.

If the 74001/2 core was inverted by the Shorty Crater impact (Bogard and Hirsch, 1978), then the relative abundance of metal spheres in the 74002 section could indicate a decrease in the formation of metal spherules and CO gas with time. The change from orange to black beads during the deposition of the volcanic beads at the Apollo 17 landing site may have occurred due to a decrease in the gas content of the magma with time. This would in turn increase the optical density in the fire fountain and inhibit cooling of the beads, favoring the formation of black beads over orange glasses (Weitz et al., 1996a). Support for this statement includes an increase in the number of compound black beads near the bottom of the core which indicates more collisions of the beads, and hence, an increase in the optical density of the fire fountain with time. Therefore, in order to explain the decrease in gas content with time, either the CO gas produced by graphite oxidation rose faster than the magma and became concentrated in the early phase of the eruption or the amount of graphite in the melt decreased with time.

5. CONCLUSIONS

The above observational and analytical data for the Apollo 17 metal blebs and volcanic beads lead to the following proposed sequence of events during ascent and eruption of magma in lunar pyroclastic eruptions (Fig. 10):

1) Formation of the $Fe_{85}Ni_{14}Co_{1.1}$ (wt%) metal spherules in the orange glass magma, presumably by oxidation of suspended graphite and a consequent reduction of iron, nickel, and cobalt oxides in the melt phase at 200 bars pressure.

2) Simultaneous or later growth of olivine phenocrysts which trapped some of the metal spherules inside or between the phenocrysts, buffering them from further reactions with the melt.

3) An event, most likely during magma ascent, that caused the metal spherules still in the orange glass magma to develop more Ni-rich rims. The irregular shape of these metal spherules and the lack of any Ni depletion in the adjacent glass indicates the apparent Ni enrichment is due to Fe loss to the surrounding melt phase by oxidation. Subsequent ascent and quenching were fast enough to preserve chemical zonation in the smaller metal blebs.

4) Explosive fire fountain eruption at the lunar surface producing submillimeter magma clasts that cooled to form either orange glasses or black beads.

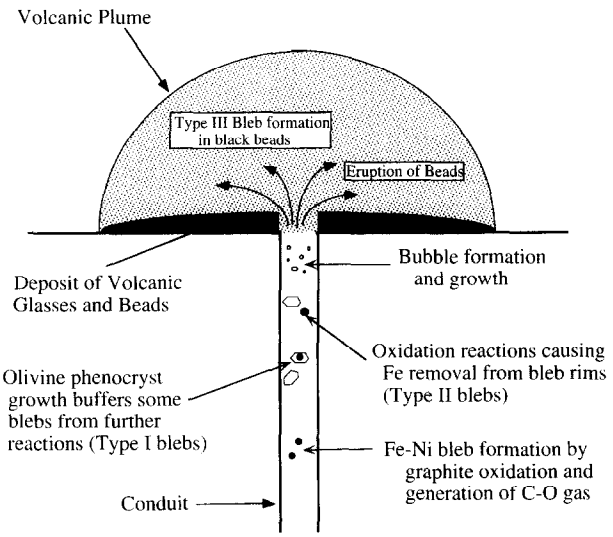

Fig. 10. Diagram illustrating the various processes occurring during ascent and eruption of the orange glass magma. At 200 bars pressure (4.0 km depth), graphite suspended in the magma is unstable and oxidizes to produce CO:CO_2 gas and Fe-Ni-Co metal blebs. Subsequent growth of olivine phenocrysts traps many of the blebs and shields them from further reactions with the melt (Type I blebs). Those blebs that remain within contact with the melt experience oxidizing reactions that remove Fe from the rims of the blebs, producing Type II blebs in volcanic beads. Finally, after eruption of the magma at the surface, slow cooling in the fire fountain volcanic gas cloud allows significant crystallization of olivine and ilmenite and the formation of Type III Fe blebs in the black beads.

5) Formation of amoeba-shaped Fe metal blebs in the black beads under reduced conditions following significant crystallization of olivine, ilmenite, and Cr-spinel. These black beads can only form in the fire fountain where the optical density is high enough to inhibit rapid cooling.

6) Deposition of the beads onto the lunar surface.

Acknowledgments—We thank J. Devine for his help with the probe analyses and B. Fogel for providing Fig. 9. This work was supported by a NASA Graduate Student Research Fellowship at Johnson Space Center for CMW (NGT-9-8), NASA Grant NAGW-3666 (MJR), and NAGW-2185 (JWH). Reviews by J. Delano and D. Lindstrom resulted in significant improvements to this manuscript.

Editorial handling: M. S. Ghiorso

REFERENCES

Arndt J. and von Engelhardt W. (1987) Formation of Apollo 17 orange and black glass beads. *Proc. 17th Lunar Planet. Sci. Conf.; J. Geophys. Res. Suppl.* **92,** E372–E376.

Blanchard D. P. and Budahn J. R. (1978) Chemistry of orange/black soils from core 74001/2. *Proc. Lunar Planet. Sci. Conf.* **IX,** 1969–1980.

Bogard D. D. and Hirsch W. C. (1978) Depositional and irradiational history and noble gas contents of orange-black droplets in the 74002/1 core from Shorty Crater. *Proc. Lunar Planet. Sci. Conf.* **IX,** 1981–2000.

Butler P. and Meyer C. (1976) Sulfur prevails in coatings on glass droplets: Apollo 15 green and brown glasses and Apollo 17 orange and black glasses. *Proc. Lunar Planet. Sci. Conf.* **VII,** 1561–1581.

Circone S. and Agee C. B. (1996) Compressibility of molten high-Ti mare glass: Evidence for crystal-liquid density inversions in the lunar mantle. *Geochim Cosmochim. Acta* **60,** 2709–2720.

Colson R. O. (1992) Solubility of neutral Nickel in silicate melts and implications for the Earth's siderophile element budget. *Nature* **357,** 65–68.

Colson R. O. (1993) Graphite solubility and CO vesiculation in basalt-like melts at one-atm. *Lunar Planet. Sci. Conf.* **XXIV,** 321–322.

Delano J. W. (1979) Apollo 15 green glass: Chemistry and possible origin. *Proc. Lunar Planet. Sci. Conf.* **X,** 275–300.

Delano J. W. (1980) Chemistry and liquidus phase relations of Apollo 15 red glass: Implications for the deep lunar interior. *Proc. Lunar Planet. Sci. Conf.* **XI,** 251–288.

Delano J. W. (1986) Pristine lunar glasses: criteria, data, and implications. *Proc. Lunar Planet. Sci. Conf.* **XVI,** D201–D213.

Delano J. W. (1990) Buoyancy-driven melt segregation in the Earth's Moon, I. Numerical results. *Proc. Lunar Planet. Sci. Conf.* **XX,** 3–12.

Dingwell D. B., O'Neill H. St. C., Ertel W., and Spettle B. (1994) The solubility and oxidation state of nickel in silicate melt at low oxygen fugacities: Results using mechanically assisted equilibrium technique. *Geochim Cosmochim. Acta* **58,** 1967–1974.

Doyle C. D. (1989) Effect of substitution of TiO_2 for SiO_2 on a_{FeO} in magma. *Geochim Cosmochim. Acta* **53,** 2631–2638.

Fogel R. A. and Rutherford M. J. (1995) Magmatic volatiles in primitive lunar glasses: I. FTIR and EPMA analyses of Apollo 15 green and yellow glasses and revision of the volatile-assisted fire-fountain theory. *Geochim Cosmochim. Acta* **59,** 201–215.

Gaddis L. R., Pieters C. M., and Hawke B. R. (1985) Remote sensing of lunar pyroclastic mantling deposits. *Icarus* **61,** 461–489.

Green D. H., Ringwood A. E., Hibberson W. O., and Ware N. G. (1975) Experimental petrology of Apollo 17 mare basalts. *Proc. Lunar Planet. Sci. Conf.* **VI,** 871–893.

Hansen P. M. (1958) *Constitution of binary alloys*. 2nd ed. McGraw-Hill Co.

Head J. W. (1974) Lunar dark-mantle deposits: Possible clues to distribution of early mare deposits. *Proc. Lunar Planet. Sci. Conf.* **V,** 207–222.

Head J. W. and Wilson L. (1989) Basaltic pyroclastic eruptions: Influence of gas-release patterns and volume fluxes on fountain structure, and the formation of cinder cones, spatter cones, rootless flows, lava ponds, and lava flows. *J. Volc. Geotherm. Res.* **37,** 261–271.

Head J. W. and Wilson L. (1992) Lunar mare volcanism: Stratigraphy, eruption conditions, and the evolution of secondary crusts. *Geochim Cosmochim. Acta* **56,** 2155–2175.

Heiken G. H. and McKay D. S. (1978) Petrology of a sequence of pyroclastic rocks from the valley of Taurus-Littrow (Apollo 17 landing site). *Proc. Lunar Planet. Sci. Conf.* **IX,** 1933–1943.

Heiken G. H., McKay D. S., and Brown R. W. (1974) Lunar deposits of possible pyroclastic origin. *Geochim Cosmochim. Acta* **38,** 1703–1718.

Hemingway B. S. (1990) Thermodynamic properties for busenite, NiO, magnetite, Fe_3O_4, and hematite, Fe_2O_3, with comments on selected oxygen buffer reactions. *Amer. Min.* **75,** 781–790.

Hess P. (1993) The ilmenite liquidus and depths of segregation for high-Ti picrite glasses. *Lunar Planet. Sci. Conf.* **XXIV,** 1285–1286.

Heyword T. R. and Goldstein J. I. (1973) Ternary diffusion in the a and g phases of the Fe-Ni-P system. *Met. Trans.* **4,** 2335–2342.

Holzheid A., Barisov A., and Palme H. (1994) The effect of oxygen fugacity and temperature on solubilities of nickel, cobalt, and molybdenum in silicate melts. *Geochim Cosmochim. Acta* **58,** 1975–1981.

Longhi J. (1987) On the connection between mare basalts and picritic volcanic glasses. *J. Geophys. Res.* **92,** E349–E360.

Longhi J. (1992) Origin of picritic green glass magma by polybaric fractional fusion. *Proc. Lunar Planet. Sci. Conf.* **XXII,** 343–353.

Meyer C., McKay D. S., Anderson D. H., and Butler P. (1975) The source of sublimates on the Apollo 15 green and Apollo 17 orange glass samples. *Proc. Lunar Planet. Sci. Conf.* **VI,** 1673–1699.

Rammensee W. and Fraser D. G. (1981) Activities in solid and liquid Fe-Ni and Fe-Co alloys determined by Knudsen cell mass spectrometry. *Ber. Bunsenges. Phys. Chem.* **85,** 588–592.

Rutherford M. J. and Fogel D. G. (1995) A15 green glass volatiles and oxidation state. *Lunar Planet. Sci. Conf.* **XXVI,** 1205–1206.

Sato M. (1976) Oxygen fugacity and other thermochemical parameters of Apollo 17 high-Ti basalts and their implications on the reduction mechanism. *Proc. Lunar Planet. Sci. Conf.* **VII,** 1323–1344.

Sato M. (1979) The driving mechanism of lunar pyroclastic eruptions inferred from the oxygen fugacity behavior of Apollo 17 orange glass. *Proc. Lunar Planet. Sci. Conf.* **X,** 311–325.

Shearer C. K. and Papike J. J. (1993) Basaltic magmatism on the Moon: A perspective from volcanic picritic glass beads. *Geochim. Cosmochim. Acta* **57,** 4785–4812.

Snyder D. A. and Carmichael S. E. (1992) Olivine-liquid equilibria and the chemical activities of FeO, NiO, Fe2O3, and MgO in natural basic melts. *Geochim. Cosmochim. Acta* **56,** 303–318.

Wasson J. T., Boynton W. V., Kallemeyn G. W., Sundberg L. L., and Wai C. M. (1976) Volatile compounds released during lunar lava fountaining. *Proc. Lunar Planet. Sci. Conf.* **VII,** 1583–1595.

Weitz C. M. and Head J. W. (1995) Lunar pyroclastic deposits: Nature and distribution of pyroclastic glasses at Taurus-Littrow. *Lunar Planet. Sci. Conf.* **XXVI,** 1485–1486.

Weitz C. M., Head J. W., and McKay D. S. (1996a) Eruption and emplacement of lunar pyroclastic glasses as inferred from the 74001/2 section. *Lunar Planet. Sci. Conf.* **XXVII,** 1411–1412.

Weitz C. M., Rutherford M. J., and Head J. W. (1996b) Oxidation states during ascent and eruption of the 74001/2 core magma. *Lunar Planet. Sci. Conf.* **XXVII,** 1413–1414.

Wilson L. and Head J. W. (1981) Ascent and eruption of basaltic magma on the Earth and Moon. *J. Geophys. Res.* **86,** 2971–3001.